STUDY ON THE BEHAVIOR OF NEEDLES AND SPRINGS FALLING FREELY IN A VISCOUS FLUID

B. Gowtham and Y.K. Suh[*]

Dept. of Mechanical Engineering, Dong-A University

점성 유체중에 자유낙하 하는 니들과 스프링의 거동에 관한 연구

고 담, 서 용 권[*]

동아대학교 기계공학과

We report in this paper the analysis of the motion of a needle and a spring in a viscous fluid under the influence of gravitational force. Lateral shift as well as vertical motion of a needle falling in a viscous fluid has been observed from a simple experiment. We also observed the combined rotation and translation of a falling spring. The trajectory and velocity of the falling needle and the spring were obtained by using an image processing technique. We also conducted numerical simulation for both problems. For the falling-needle problem, we employed a theory; but it turns out that significant correction is required for the solutions to match the numerical and experimental data. For the falling spring problem various theoretical formula were tested for their justification, but none of the existing theories can successfully predict the numerical and experimental results.

Nomenclature

a : Radius of the wire of needle and spring

B : Dimensionless parameter; $[1+(3C_wL^+/2)G^+]/[1+2/(3L^+)]$

b : Radius of container

b^+ : Dimensionless gap factor (b/a)

C_n, C_s : Coefficient for the normal and tangential components of the drag force.

C_w : Constant, $1.003852-1.961010k+0.957095k^2$

D_m : Mean diameter of spring

F_b, F_G : Buoyancy and gravity force

F_D : Viscous drag force and their components

F_{gb} : Effective gravitational force

F_n, F_s : Normal and tangential components of force

G^+ : Dimensionless geometric factor, $[k^2(1-\ln k)-\ln k+1]/(1-k^2)$

k : Ratio of needle to the container radius

$\boldsymbol{k}$: Unit vector downward

K_n, K_s : Correction factors for the normal and tangential force components

L : Material length of the spring and needle

L_a : Axial length of the spring

L^+ : Ratio of needle length to diameter, $L/(2a)$

Q^+ : Dimensionless flow rate, $Q/(\pi a^2 U_\infty)$

RFT : Resistive force theory

r : Radial coordinate

r_c : Mean radius of spring

$\boldsymbol{r}_c$: Mean radius vector of spring

r^+ : Dimensionless radial distance

U_t : Terminal velocity of needle and spring

u : Translational velocity of spring

u^+ : Dimensionless velocity

α : Lateral shift of the needle
γ : Helix angle of spring
θ : Initial angle of the needle
λ : Pitch of spring
μ_f : Dynamic viscosity of fluid
ρ_f : Density of fluid
ρ_s : Density of solid
ω : Angular velocity of needle

1. Introduction

The Propulsion of microorganisms by flagella motion has been a subject of considerable interest, especially in the period from 1950s to the 1970s when slender body theory for Stokes flow was developed. The work of Gray and Hancock[1] formed the foundation of the widely accepted resistive force theory, which provides a simple analytical method for calculating the swimming speed and thrust produced by the flagella motion[2].

A renewed interest in low Reynolds number propulsion has emerged in recent years due to the growing attention to bio-mimetics that has opened up the prospect of many new bio-robotic applications[3]. Development of effective devices of this kind requires a better understanding of propulsion at low Reynolds numbers, and even today the number of experimental studies on low Reynolds number propulsion is very limited.

Recent findings from microfluidic studies have provided novel insights on the fundamental mechanisms by which a bacterium propels in a viscous fluid. Such insights helped the microfluidic technology to use the bio-molecular motors from flagellated bacteria as fluidic actuators to generate fluid motion in a microfluidic network and artificial swimming micro robot for biomedical applications[4].

Creation of thrust force due to the rotation of a spring, mimicking the rotating flagella, is obviously the foundation of the propulsion of microorganisms. In this case, the rotation of the surrounding fluid corresponds to the primary motion, whereas the axial motion corresponds to the secondary one. However, precise measurement of the force requires a sophisticated experimental facility and sensors. In this study, therefore, we contrive the reverse situation, in which the axial force is provided by the gravitation and the spring's axial (primary) and rotational (secondary) motions are
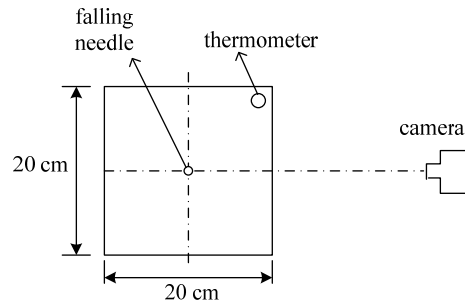

Fig. 1 Top view of the experimental setup

measured by image processing techniques, which is much easier than the original configuration. We aim in this study to confirm our understanding of the mechanism of the spring's motion and the validity of the relevant theoretical formula reported in the literature to estimate the spring's motions. Since the total drag force acting on the spring can be considered as the line integral of the force density (force per unit length) acting on the small element of the spring, the situation of a falling needle is thought to be a more fundamental model.

Here we report the results obtained from experiment, numerical and theoretical studies on the motion of two kinds of objects, i.e., a helical spring and cylindrical needle. The present study focuses on the creeping flow over those objects falling freely in viscous fluid under the influence of gravity. Two kinds of theoretical approaches, the theory proposed by Park and Irvine[5,6] and Kim et al.[7] and the classical resistive-force theory were used to determine the motion of the needle and spring. Numerical calculations were also carried out using a commercial code (Ansys CFX V13.0). The reason for the lateral shift of needle during the travel in the viscous fluid (glycerol) is explored. Finally the optimum helix angle of the spring at which it produces maximum velocity ratio (ratio of the rotating velocity and the falling velocity) was evaluated from the numerical and theoretical analysis.

2. Experiment

The schematic of the experimental apparatus for a needle and a spring falling in a tank is shown in Fig. 1. The needle used for the experiment has dimensions, $L_a = 4$ cm and $a = 0.5$ mm (and 0.25 mm). The spring
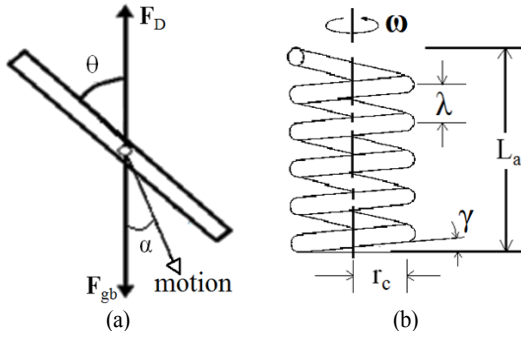
Fig. 2 Schematic of the needle (a) and spring (b)

has dimensions of $r_c = 2.375$ mm, $a = 0.125$ mm and $\gamma = 45°$ (and 31°) with an axial length of $L_a = 4$ cm. The helix angle of springs are calculated using the relationship given by

$$\tan\gamma = \frac{\lambda}{2\pi r_c} \tag{1}$$

Pure synthetic glycerol (90%, Samchun Pure Chemicals Co., Ltd) was used as the working fluid and its level was maintained at 20 cm. The temperature of the fluid was maintained at 22°C~23°C, which was measured using a standard thermometer just prior to the experiment. Viscosity of the fluid at different temperatures is measured separately from a falling-ball-viscometer experiment, which agreed well with the empirical data of Cheng[9]. The Reynolds number, $Re = 2\rho_f U_t a / \mu_f$, based on the fluid density ρ_f, viscosity μ_f, the terminal velocity U_t and the material diameter of the spring or the needle a turns out to be low enough for the Stokes flow approximation to be valid; using $\rho_f = 1262$ kg/m³ and $\mu_f = 1.074$ Ns/m², we get $Re = 0.6$ for $a = 0.5$ mm and typical value $U_t = 5$ cm/s, and $Re = 0.009$ for $a = 0.25$ mm and typical value $U_t = 1.5$ cm/s.

Terminal falling velocity, lateral shift of the needle and rotational velocity of the spring were calculated by using an image processing technique for the images recorded from a camera.

3. Analytical Procedure

The schematic of the force balance for the needle falling under the gravity is given in Fig. 2(a); the same principle applies to the falling spring problem.

The terminal velocity and rotational velocity of the needles and springs were obtained from the force balance equation,

$$F_D = F_{gb} \equiv F_g - F_b \tag{2}$$

which is adopted in the theory proposed by Park and Irvine[5,6] and Kim et al.[7] for the needle and the resistive-force theory[1,11-13] for the spring. These theoretical methods were employed to estimate the terminal and rotational velocities of needles and springs.

3.1. Needle falling inclined to the vertical axis

A general formulation for the effective gravitational force, F_{gb}, and the formula for drag force, F_D, for the needle falling vertically ($\theta = 0^o$) are given as

$$F_{gb} = \pi a^2 g (\rho_s - \rho_f) L_a \tag{3}$$

$$F_D = 2\pi \mu_f U_t L_a B \left(\frac{\partial w^+}{\partial r^+} \right) \tag{4}$$

where, $(\partial w^+ / \partial r^+)$ is the dimensionless shear stress and B is a dimensionless factor (given in the nomenclature).

For the needle falling normal to the system axis ($\theta = 90^o$), the drag force is given by

$$F_D = \frac{4\pi \mu_f U_t L_a}{2 - \ln(Re)} \tag{5}$$

The terminal velocity of the falling needle, U_t, is calculated by equating Eq. (3) and (4) for $\theta = 0^o$, and Eq. (3) and (5) for $\theta = 90^o$ according to Eq. (2).

When the needle falls making an arbitrary angle θ with respect to the vertical axis [see Fig. 2(a)], the drag force $\mathbf{F}_D$ must be considered to be a vectorial sum of the normal component F_{Dn} and the tangential component F_{Ds}, which are given as

$$F_D = \frac{K_n 4\pi \mu_f U_t L_a \sin(\theta - \alpha)}{2 - \ln[2\rho_f a U_t \sin(\theta - \alpha) / \mu_f]} \tag{6}$$

$$F_{Ds} = K_s 2\pi \mu_f U_t \cos(\theta - \alpha) B L_a \left(\frac{\partial w^+}{\partial r^+} \right)_{r^+ = 1} \tag{7}$$

Here, the correction factors K_n and K_s were calculated from Eq. (6) and (7) with the terminal velocity data

obtained from the experiment for the two extreme cases, $\theta = 0^o$ and $\theta = 90^o$. The needle falls down showing a lateral shift when it is inclined to the system axis. The two unknowns U_t and α are obtained from the two requirements that the vertical component of $\boldsymbol{F}_D$ is equal to F_{gb} and the horizontal component is zero.

3.2. Combined translation and rotation of a spring

A common way to study the interaction of the helix with its flow field is using the slender body theory that employs a Green function approach for the solution of Stokes equation. The disadvantage of this method is its computational expense[10]. This is the reason why we use in this work the resistive force theory which is also a common technique to study the dynamics of elastic filaments which compose the spring in a viscous fluid. In this theory, local friction coefficients per unit length parallel and perpendicular to the tangential vector of the filament were used.

Consider a rigid filament segment of unit length showing the translational velocity $\boldsymbol{u}$ and angular frequency $\boldsymbol{\omega}$. The segment moves with a combined translational and rotational velocity $\boldsymbol{v} = (\boldsymbol{u} + \boldsymbol{\omega} \times \boldsymbol{r}_c)$, where $\boldsymbol{u} = U_t \boldsymbol{k}$ is the terminal linear velocity ($\boldsymbol{k}$ is the unit vector downward), $\boldsymbol{\omega} = \omega \boldsymbol{k}$ is the angular velocity vector of the spring and $\boldsymbol{r}_c$ is the radial vector (see Fig. 2(b)).

In resistive force theory, the force per unit length exerted by the fluid is proportional to the local centerline velocity $\boldsymbol{v}$. The key element here is that the multiplying coefficient is however not identical to each other. Decomposing $\boldsymbol{v}$ into the normal and tangential components to the body centerline, v_n and v_s, we can write the two components of force per unit length as

$$F_s = \mu_f C_s v_s \tag{8}$$

$$F_n = \mu_f C_n v_n \tag{9}$$

In this paper, theoretical results of the velocity obtained with the coefficients of resistance proposed by various researchers for computing flagella motions were compared with each other and they are listed below. Firstly,

$$C_s = \frac{2\pi}{\ln(2\lambda/a) - 0.5} \tag{10a}$$

$$C_n = \frac{4\pi}{\ln(2\lambda/a) - 0.5} \tag{10b}$$

which were proposed by Gray and Hancock[1]. Cox[11] and Johnson and Brokaw[12] proposed the following forms.

$$C_s = \frac{2\pi}{\ln(2\lambda/a) - 0.5} \tag{11a}$$

$$C_n = \frac{4\pi}{\ln(2\lambda/a) + 0.5} \tag{11b}$$

In 1976, Lighthill[13] suggested the following.

$$C_s = \frac{2\pi}{\ln(2q/a)} \tag{12a}$$

$$C_n = \frac{4\pi}{\ln(2q/a) + 0.5} \tag{12b}$$

where $q = 0.09\lambda$. This study also considers a combined expression of resistance coefficients where the tangential coefficient C_s is taken from Eq. (10a) and the normal coefficient C_n from Eq. (12b).

The equations for the two unknowns, U_t and ω, are given as

$$F_n \cos\gamma + F_s \sin\gamma = F_{gb} \tag{13a}$$

$$F_n \sin\gamma - F_s \cos\gamma = 0 \tag{13a}$$

which were solved iteratively by using the standard Gauss-Seidel solver.

4. Numerical Scheme

Numerical simulation of the Navier-Stokes equations for the motion of the falling needle and spring was conducted using a commercial code (Ansys CFX V13.0). The continuity and momentum equations are:

$$\nabla \cdot \boldsymbol{u} = 0 \tag{14}$$

$$\rho_f \frac{\partial \boldsymbol{u}}{\partial t} + \rho_f(\boldsymbol{u} \cdot \nabla)\boldsymbol{u} = -\nabla p + \mu_f \nabla^2 \boldsymbol{u} \tag{15}$$
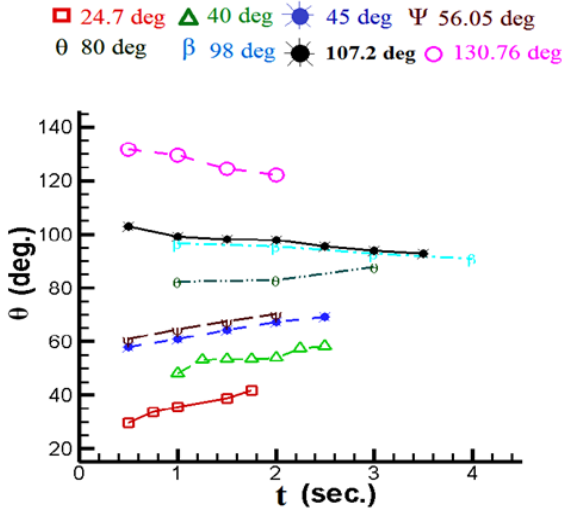
Fig. 3 Instantaneous variation of needle angle, θ, with various orientations for $L^+ = 40$
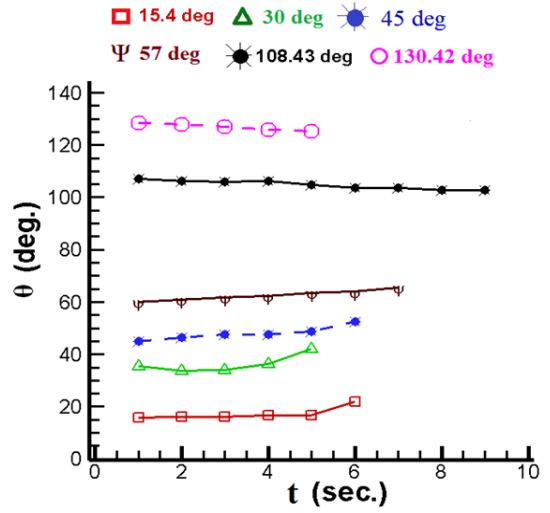

Fig. 4 Instantaneous variation of needle angle, θ, with various orientations for $L^+ = 80$

In reality, the needle falls down with a lateral shift. The spring also falls down with rotation. To simulate those real situations, however, we need moving grids which may bring forth another source of numerical errors. We in this study therefore consider the relative motion of the fluid while the needle and spring are kept stationary. The vertical terminal velocity U_t and the lateral shift velocity of the needle is determined from the requirement of force balance as discussed in section 3. Similarly, U_t and ω of the spring is determined from the force balance, too.

5. Result and Discussion on a Falling Needle

Needles in general tend to shift laterally when they fall through the fluid after they are dropped with $\theta \neq 0^o$ or $\theta \neq 90^o$. Moreover, it turned out that θ varies with time while the needle is falling.

The instantaneous variation of θ with time at several initial orientations to the system axis was obtained from the experiment as shown in Fig. 3 for $L^+ = 40$ and Fig. 4 for $L^+ = 80$.

The figures reveal that regardless of the initial angle of the needle, value of θ tends to 90°. Obviously it is caused by the effect of the bottom wall of the container; apparently the needle always arrive at the bottom with $\theta = 90^o$. Another reason lies in the fact that the stagnation

point of the flow near the leading edge of the needle is located on the bottom side whereas that near the trailing edge is located on the top side of the needle, respectively. As is well known, the pressure near the leading stagnation point is always higher than that near the trailing stagnation point in stokes flow, and thus we expect that the resultant restoring torque tends to make the needle to align horizontally.

We can also see from Fig. 3 and 4 that the needle with $L^+ = 40$ shows faster variation of θ in time than with $L^+ = 80$. This is mainly due to the fact that the two needles have the same length but the diameter of the former is twice the latter so that the needle with $L^+ = 40$ falls faster; it can be shown from Eq. (3) and (4) that the velocity is directly correlated with the square of the needle radius (a^2).

Experimental results of U_t obtained from the numerical, theoretical and experimental methods are presented in Fig 5(a) and 5(b). The theoretical results are given from the principle of force equilibrium described with Eq. (6) and (7) and thereafter; the two coefficients K_n and K_s are determined from the matching of the terminal velocity between the theory and experiment for the case of $\theta = 0^o$ and $\theta = 90^o$, respectively. The overall dependence of the terminal velocity on the inclination angle is well reproduced by the theory. We can also see that the needle falling with its axis parallel to the system axis ($\theta = 0^o$, Fig. 5(a)) shows a higher velocity than the one falling
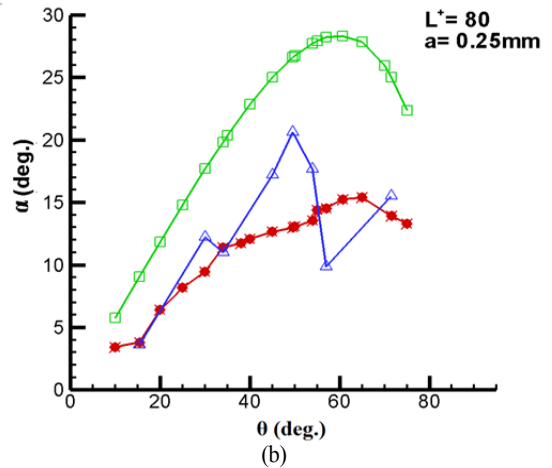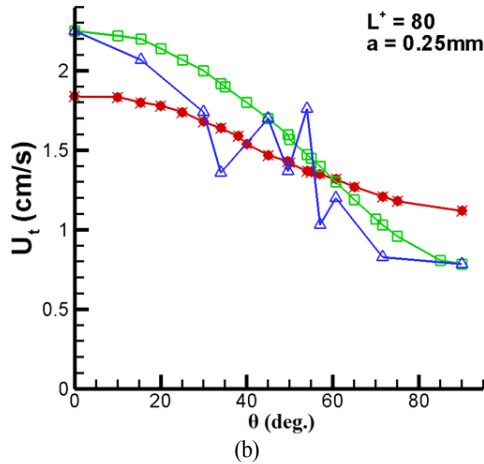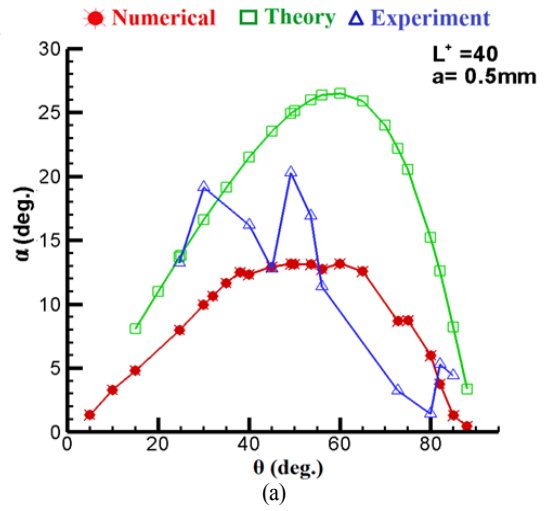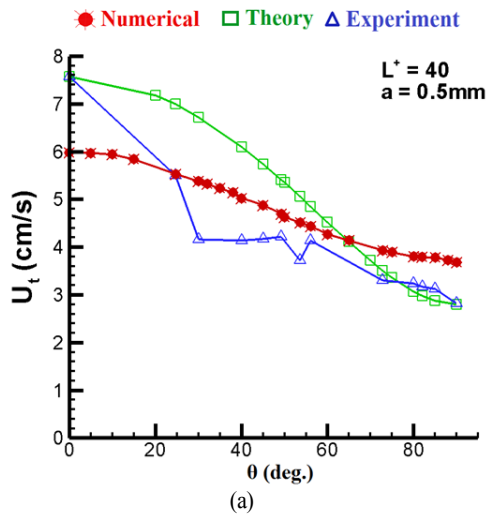
Fig. 5 Comparison of the terminal velocity of the needles obtained from numerical, analytical and experimental measurement for (a) $L^+ = 40$ and (b) $L^+ = 80$

Fig. 6 Comparison of the lateral-shifts of the needle obtained from numerical, analytical and experimental measurement for (a) $L^+ = 40$ and (b) $L^+ = 80$

normal to the axis ($\theta = 90^o$, Fig. 5(b)) indicating that the viscous drag force acting on the needle caused by the normal component of the fluid velocity is higher than that caused by the tangential component.

As a consequence of such difference in the drag force, in the angle θ between $\theta = 0^o$ and $\theta = 90^o$, we can expect that the falling needle should tend to move to the direction experiencing a smaller drag force, i.e., parallel to the needle axis, which is called lateral shift.

The data of the lateral shift are presented in Fig 6(a) and 6(b). The theoretical data show that regardless of the dimensions of the needle, the angle α representing the lateral shift shows maximum values between 25° and 30° at the needle angle θ in the range $55^o \leq \theta \leq 65^o$. The numerical and experimental data, however, reveal reduced α values, less than 20°. Because of the data scattering, the range of θ for the maximum lateral shift cannot be provided from the experimental results. The numerical results give approximately $\theta = 55^o$ for $a = 0.5$ mm and $\theta = 65^o$ for $a = 0.25$ mm for the maximum lateral shift. The existence of such lateral shift in the falling needle is considered to be a basic mechanism of the self-rotation of a falling spring.
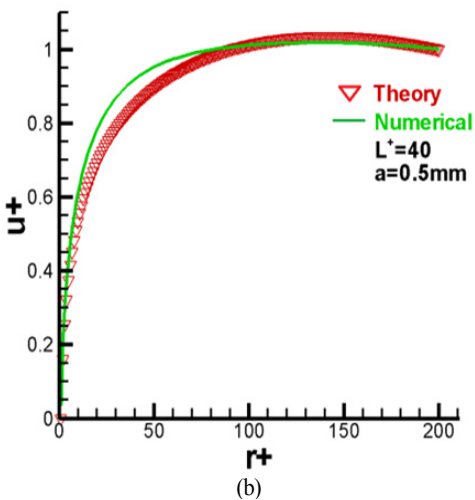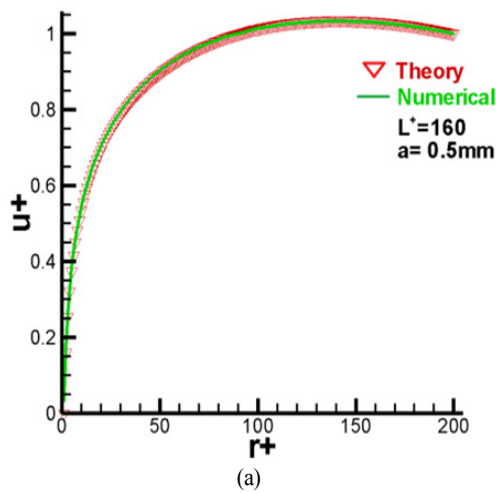
(a)

(b)

Fig. 7 Comparison between the theoretical and numerical results of terminal velocity for the case of vertically falling needle at two values of dimensionless length factor L^+

(a)

(b)

Fig. 8 Contours of (a) axial velocity and (b) pressure near the falling spring of helix angle $\gamma = 45^o$

Fig. 7 reveal that the larger needle length indeed yields a better agreement between the theory and numerical solutions validating the argument given above.

6. Results and Discussions on a Falling Spring

We now present the results of the numerical, analytical and experimental studies on a falling spring.

Shown in Fig. 8 are the contours of the velocity and pressure. From Fig. 8(a), we notice that the velocity inside the spring is overall less than the free stream velocity which is due to the hydrodynamic interaction among coils of wires[3]. The pressure distribution of Fig. 8(b) is in line with the physical observation in low-Reynolds-number flows, i.e., high and low pressure near the leading and trailing stagnation points, respectively.

Comparison among the experimental, numerical and theoretical solutions of the terminal velocity U_t and the rotational velocity $r_c\omega$ for the springs with various helix angles are given in Fig. 8 and 9. Here five kinds of analytical formula are employed in obtaining the theoretical

The discrepancy between the numerical (or experimental) and analytical solutions in the terminal velocity and lateral shift angle is mainly due to the fact that the theory is based on the one-dimensional axis-symmetric configuration of the problem while the actual set-up is three-dimensional. For the case of vertically falling needle, for instance, the one-dimensional axis-symmetric velocity profile is possible only when the needle is infinitely long or the gap between the container and the needle is very small. The effect of the tank wall should be more pronounced in determining the lateral-shift motion.
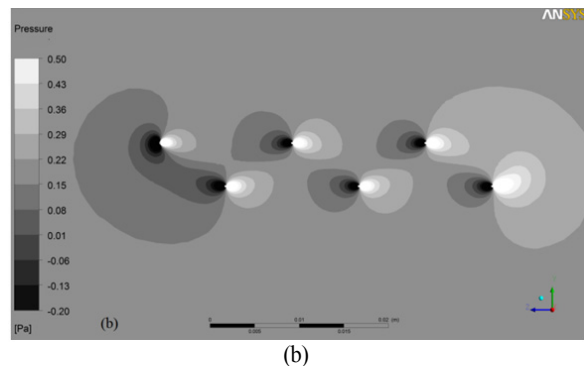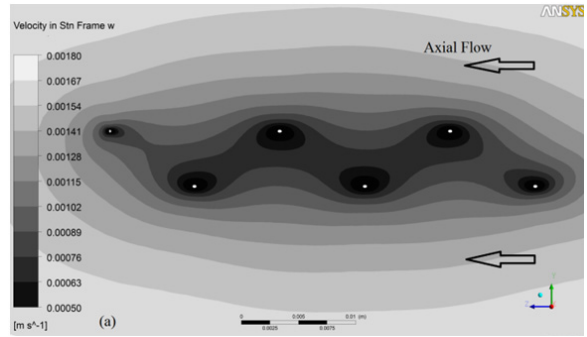
-- Kim et al. [7] (with no correction factors)
△ Park and Irvine [5] (with correction factors)
--- Combination of (10a) and (12b)
□ Cox [11], Johnson & Brokaw [12]
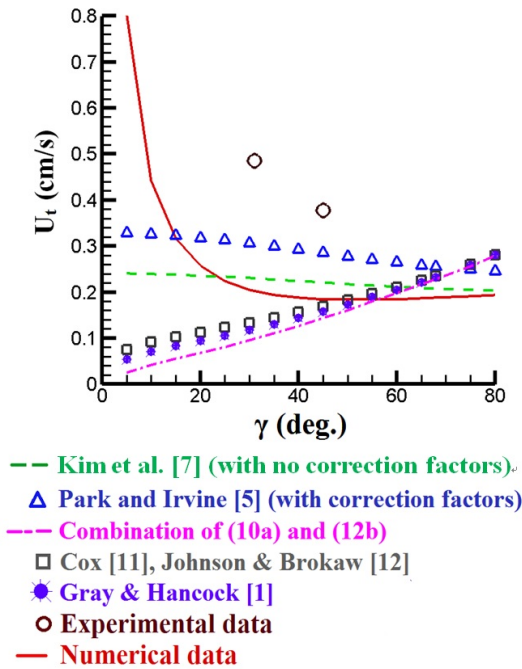✳ Gray & Hancock [1]
○ Experimental data
— Numerical data

Fig. 9 Comparison of the Terminal velocity data obtained from experimental, numerical and theoretical calculations for the springs with various helix angles and having the following dimensions; $L = 4$ cm, $D_m = 4.75$ mm, and $d = 0.25$ mm
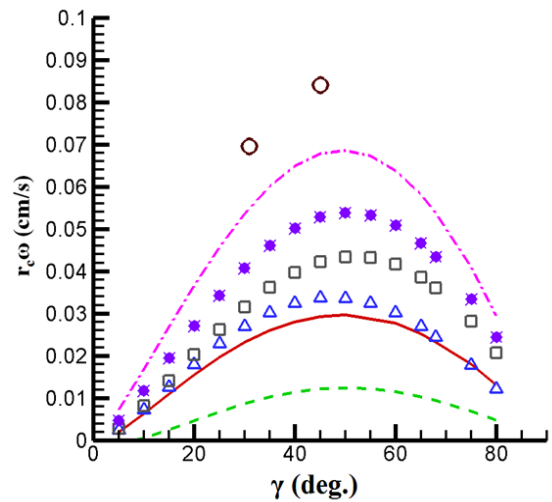

Fig. 10 Comparison of the rotational velocity data obtained from experimental, numerical and theoretical calculations for the springs with various helix angles and having the following dimensions; $L = 4$ cm, $D_m = 4.75$ mm, and $d = 0.25$ mm (description on the symbols is the same as in Fig. 8)

data and the experimental data are obtained only for two helix angles.

In Fig. 9 we can see that among the data for the terminal velocity, those obtained from the theory of Park and Irvine[5] and Kim et al.[7] shows a relatively close agreement with the experimental data. In overall, however, none of the theories or numerical data can fit the experimental data satisfactorily. In particular at helix angles close to zero, the discrepancy is more significant.

Fig. 10 shows comparison among the experimental, numerical and theoretical solutions of the rotational velocity of the springs with various helix angles. The experimental data are higher than any other results, among which, the solutions obtained from the theory combining Eq. (10a) and (12b) yield a closer agreement with the experimental data.

In Fig. 10, however, all the theoretical predictions follow the same trend; that is, the rotational velocity tends to zero at $\gamma = 0^o$ and $\gamma = 90^o$ and it becomes maximum at the critical angle around $\gamma = 50^o$. We can see that the critical angle for the spring, at which the rotational velocity is maximized, is very close to the critical angle

of inclination of a falling needle showing the maximum lateral shift as shown in Fig. 6. This indicates that rotation of the falling spring should be related to the lateral shift of the needle. Thus, we can say that rotation of the falling spring is caused by the fact that the normal component of the fluid drag force acting on the wire is larger than the tangential component. Fig. 10 also reveals that the theoretical data given by Park and Irvine[5] with correction factors show the best agreement with the numerical ones.

Our prediction of the critical helix angle of the spring seems to be in close relation to the critical helix angle of the spring ($45^o \leq \gamma \leq 55^o$) showing the maximum thrust as predicted by Zhong et al.[3].

There are discrepancies among the numerical, experimental and theoretical data as shown in Fig. 9 and 10. We assume that two factors not considered in RFT are the main reason for the discrepancy in particular between the numerical and theoretical results; the hydrodynamic interactions between the helical loops of the spring and the end effect as reported by Zhong et al.[3].

We notice from Fig. 9 that the theoretical terminal velocity is much smaller than the numerical one at low helix angles. This may be understood from the fact that at small helix angles the fluid drag force should be smaller than the theory, which is not considered in the theory

(e.g., Gray and Hancock[1] and Lighthill[13]). Thus we expect a faster falling motion of the spring than the theory predicts for small helix angles, which is in line with the data shown in Fig. 9. On the other hand, at large helix angles close to 90°, the numerical results of the terminal velocity are smaller than the theoretical prediction. At high helix angles, the number of turns of spring coil is small and thus the end effect of the spring, which is also not considered in the theory, should be more relevant leading to a higher drag force. Thus the theoretical results are expected to be larger than the numerical ones for high helix angles as shown in Fig. 9.

7. Conclusions

In this work free falling motion of needles and helical springs was studied by using experiment, numerical simulation and theoretical analysis with an ultimate purpose of understanding the propulsion mechanism of microorganisms with flagella in bio-fluids as the springs were considered as the macroscopic model of the actual flagella.

We can list up important outcomes of our research work as follows

(1) The terminal velocity data of needles clearly show that the needle vertically oriented falls faster than the one horizontally oriented.

(2) The lateral shift occurs in the motion of a falling needle its magnitude being dependent upon the orientation of the needle, and the maximum lateral shift occurs for the needle falling at the angle θ in the range $55^o \leqq \theta \leqq 65^o$.

(3) The reason for the discrepancy between the numerical and analytical solutions for the motion of needles is due to the idealized assumption of an infinitely long needle so that the problem becomes axi-symmetric and one-dimensional which is obviously contrary to the actual situation.

(4) The theoretical terminal velocity of springs is much smaller at low helix angles than the numerical data especially at $\gamma \leqq 40^o$, which is understood from the fact that at small helix angles the hydrodynamic interaction between neighboring coils actually becomes larger and thus the theory over-predicts the fluid drag force.

(5) In the distribution of the rotational velocity versus the helix angle, both the numerical and theoretical predictions follow the same trend; that is, the rotational velocity tends to zero at the helix angle $\gamma = 0^o$ and $\gamma = 90^o$ and it becomes maximum at the critical angle around $\gamma = 50^o$.

(6) Most of the theoretical data (especially RFT) for the terminal velocity and rotational velocity of springs deviate from the numerical and experimental data, because of the hydrodynamic interaction between the helical coils and the end effect as addressed in Zhong et al.[3].

Note

This paper is a revised version of the paper presented at the KSCFE 2013 Fall Conference, Seoul, Korea, Oct. 31 ~ Nov. 1, 2013.

References

[1] 1955, Gray, J. and Hancock, G.J., "The propulsion of sea-urchin spermetazoa," *J. Exp. Biol.*, Vol.32, pp.802-814.

[2] 1971, Chwang, T. and Wu, T.Y., "A note on the helical movement of micro-organisms," *Proc. Roy. Soc. London B.*, Vol.178, pp.327-346.

[3] 2013, Zhong, S., Moored, K.W., Victor, P., Garcia-Gonzalez, J. and Smits, A.J., "The flow field and axial thrust generated by a rotating rigid helix at low Reynolds numbers," *Exp. Thermal and Fluid Sci.*, Vol.46, pp.1-7.

[4] 2012, Ranjith, M., Numerical study on bacterial flagella motion and bundling using an immersed boundary method, Dissertation submitted to the Graduate School, Dong-A University, Korea.

[5] 1984, Park, N.A. and Irvine Jr, T.F., "The falling needle viscometer: A new technique for viscosity measurements," *Wärme-und Stoffübertragung*, Vol.18, pp.201~203.

[6] 1995, Park, N.A. and Irvine Jr, T.F., "Falling cylinder viscometer and end correction factor," *Rev. Sci. Instrum.*, Vol.66. No.7, pp.3982~3984.

[7] 1994, Kim, I., Irvine Jr, T.F. and Park, N.A., "Experimental study of the velocity field around a falling needle viscometer," *Rev. Sci. Instrum.*, Vol.65, No.1, pp.224~228.

[8] 1994, Gui, F. and Irvine Jr, T.F., "Theoretical and experimental study of the falling cylinder viscometer," *Int. J. Heat Mass Transfer*, Vol.37, Suppl.1, pp.41～50.

[9] 2008, Cheng, N.S., "Formula for viscosity of glycerol-water mixture," *Ind. Eng. Chem. Res.*, Vol.47, pp.3285~3288.

[10] 2012, Vogel, R., The bacterial flagellum: Modeling the dynamics of the elastic filament and its transition between polymorphic helical forms, Dissertation submitted to Universität Berlin.

[11] 1970, Cox, R.J., "The motion of long slender bodies in a viscous fluid. Part 1, General theory," *J. Fluid Mech.*, Vol.44, No.4, pp.791-810.

[12] 1979, Johnson, R.E., Brokaw, C.J., "Flagella hydrodynamics: A comparison between resistive force theory and slender body theory," *Biophysics. J.*, Vol.25, pp.113-127.

[13] 1976, Lighthill, J., "Flagella hydrodynamics," *Soc. Ind. Appl. Math. Rev.*, Vol.18. No.2, pp.161-230.